AIAA JOURNAL
Vol. 39, No. 2, February 2001

Bayesian Modal Updating by Use of Ambient Data

Lambros S. Katafygiotis,* Ka-Veng Yuen,† and Jay-Chung Chen‡
Hong Kong University of Science and Technology, Clear Water Bay, Hong Kong, People's Republic of China

The problem of identification of the modal parameters of a structural model by using measured ambient response time histories is addressed. A Bayesian probabilistic framework for modal updating is adopted, which allows one to obtain not only the optimal (most probable) values of the updated modal parameters but also their uncertainties, calculated from their joint probability distribution. Calculation of the uncertainties of the identified modal parameters is very important if one plans to proceed with the updating of a theoretical finite-element model based on modal estimates. A new probabilistic approach is proposed that uses the statistical properties of an estimator of the spectral density to obtain expressions for the updated probability density function (PDF) of the modal parameters. The proposed approach is first introduced for single-degree-of-freedom systems and then extended for multiple-degree-of-freedom systems. It is found that the updated PDF can be well approximated by a Gaussian distribution centered at the optimal parameters at which the posterior PDF is maximized. Examples using simulated data are presented to illustrate the proposed method.

Nomenclature

$\boldsymbol{a}$	=	parameter vector for identification
$\boldsymbol{C}$	=	damping matrix
$f(t)$	=	Gaussian white noise excitation
$h(t)$	=	impulse response function
INT	=	integer part of a real number
$\boldsymbol{K}$	=	stiffness matrix
$\boldsymbol{L}_0$	=	observation matrix
$\boldsymbol{M}$	=	mass matrix
N_d	=	number of degrees of freedom
N_m	=	number of modes considered
N_s	=	number of measured degrees of freedom
$n_x(t)$	=	measurement noise
$q(t)$	=	generalized coordinate
$R(t)$	=	autocorrelation function
S_{f0}	=	spectral intensity of white noise excitation
S_{nx0}	=	spectral intensity of measurement white noise
$S(\omega)$	=	spectral density function
tr	=	trace of a matrix
$\hat{\boldsymbol{X}}_N$	=	measured response vector
Δt	=	sampling time interval
ζ	=	damping ratio
$\boldsymbol{\Phi}$	=	modeshape matrix
ω_0	=	natural frequency in rad/s

I. Introduction

THE problem of identification of the modal parameters of a linear structural model by using dynamic data has received much attention over the years because of its importance in model updating, response predictions, structural control, and health monitoring. Many methodologies have been formulated, both in the time and frequency domain, for the case in which the input excitation has been measured.[1] For example, in the aerospace industry, modal tests are performed on extensively instrumented spacecrafts by using precisely controlled excitations for determining the modal parameters such as natural frequencies, dampings, and modeshapes.[2–4] Here, the objective is to verify the mathematical model to be used in loads analysis by comparing the modal parameters obtained from the modal tests to those from the mathematical models. In Ref. 5, a statistical methodology was presented to identify the structural parameters from the modal parameters.

Much attention has also been devoted to the identification of modal parameters in the case in which no input but only response measurements are available. In particular, a lot of effort has been devoted to the case of free vibrations or impulse response and to the case of ambient vibrations. In the former case, often time-domain methods based on autoregressive moving average (ARMA) models are utilized; using least squares as an integral part of their formulation. It has been found that the least-squares method[6] yields biased estimates. A number of methods have been developed to eliminate this bias. A comparison of such methods can be found in Ref. 7.

The case of ambient vibration surveys (AVSs) have attracted much interest because AVSs offer a means of obtaining dynamic data in an efficient manner, without requiring the setup of special dynamic experiments, which are usually costly, time consuming, and often obtrusive. In an AVS the naturally occurring vibrations of the structure (from wind, traffic, or microtremors) can be measured, and system identification techniques can be used to identify the small-amplitude modal frequencies and modeshapes of the lower modes of the structure. The assumption usually made is that the input excitation is a broadband stochastic process adequately modeled by white noise. Many time-domain methods were developed to tackle this problem. One such method is the random decrement (RD, or Randomdec) technique,[8] which is based on curve fitting of the estimated RD functions corresponding to various triggering conditions. It can be shown that the theoretical RD functions can be expressed as a linear combination of the correlation functions and their derivatives. Several methods are based on fitting directly the correlation functions, using least-squares type of approaches.[9] Different ARMA-based methods have been proposed, such as, for example, the two-stage least-squares method.[10] The prediction error method[11] utilizes the Kalman filter[12] to obtain the modal parameters. Methods for treating nonlinear systems have also been investigated.[13]

Besides the above time-domain approaches, many frequency-domain approaches were developed and have also been widely used. Some examples of frequency-domain approaches are complex curve fitting,[14] the pole/zero assignment technique,[15] the simultaneous frequency-domain approach,[16] the orthogonal polynomial approach,[17] the polyreference frequency-domain approach,[18] the multireference simultaneous frequency-domain approach,[19] and the best-fit reciprocal vectors method.[20]

The results of modal identification are usually restricted to the "optimal" estimates of the modal parameters. However, there is additional information related to the uncertainty associated with the above estimates that is valuable for further processing. For example, in the case in which the results of the modal identification are used to update the theoretical finite-element model of a structure, the updating procedure usually involves the minimization of a positive-definite quadratic function involving the differences between the theoretical and identified experimental modal parameters.

Received 23 April 1999; revision received 25 June 2000; accepted for publication 26 June 2000. Copyright © 2000 by the American Institute of Aeronautics and Astronautics, Inc. All rights reserved.

*Associate Professor, Department of Civil Engineering; lambros@ust.hk.
†Graduate Student, Department of Civil Engineering; kvyuen@ust.hk.
‡Professor, Department of Mechanical Engineering; jchen@ust.hk. Associate Fellow AIAA.

The weighting matrix in this objective function should reflect the uncertainties in the values of the identified modal parameters and should be chosen to be equal to the inverse of the covariance matrix of these parameters. In practice, usually this covariance matrix is estimated by calculating the statistics of the optimal estimates of the modal parameters obtained from several sets of ambient data.

In this work a Bayesian probabilistic approach is developed for determining the uncertainties of the modal estimates in an AVS. A Bayesian probabilistic system identification framework has been presented for the case of measured input.[21] For ambient vibration data, the Bayesian approach proposed herein is based on the statistics of an estimator of the spectral density. The proposed approach allows for the direct calculation of the probability density function (PDF) of the modal parameters, which can then be approximated by an appropriately selected multivariate Gaussian distribution. The formulation is first presented for single-degree-of-freedom (SDOF) systems and then extended to multiple-degree-of-freedom (MDOF) systems.

II. Mathematical Formulation

A. Single-Degree-of-Freedom Case

Consider the SDOF oscillator with an equation of motion:

$$\ddot{x} + 2\zeta\omega_0\dot{x} + \omega_0^2 x = f(t) \tag{1}$$

where ω_0 and ζ are the natural frequency and damping ratio of the oscillator, respectively, and $f(t)$ is Gaussian white noise with spectral density $S_f(\omega) = S_{f0}$.

It is known[22] that for given system parameters, the response $x(t)$ is a Gaussian process with zero mean, autocorrelation function

$$R_x(\tau) = \left(\pi S_{f0}\Big/2\zeta\omega_0^3\right)\exp(-\zeta\omega_0|\tau|)\Big[\cos(\omega_{0D}|\tau|) + \zeta\Big/\sqrt{1-\zeta^2}\sin(\omega_{0D}|\tau|)\Big] \tag{2}$$

and spectral density function

$$S_x(\omega) = S_{f0}\Big/\Big[\left(\omega^2 - \omega_0^2\right)^2 + (2\zeta\omega\omega_0)^2\Big] \tag{3}$$

where $\omega_{0D} = \omega_0\sqrt{(1-\zeta^2)}$ is the damped frequency of the oscillator.

Assume discrete data, with time step Δt, and let $\hat{x}(m)$ describe the measured response at time $t = m\Delta t$. Also, assume that as a result of measurement noise and modeling error there is a difference between the measured response $\hat{x}(m)$ and the model response $x(m)$, which can be adequately represented by a discrete white noise process $n_x(m)$ with zero mean and variance σ_{nx}^2. That is,

$$\hat{x}(m) = x(m) + n_x(m), \qquad m = 0, \ldots, N-1 \tag{4}$$

where n_x has spectral density

$$S_{nx}(\omega) \equiv S_{nx0} = (\Delta t/2\pi)\sigma_{nx}^2 \tag{5}$$

Let $\boldsymbol{a} = [\omega_0, \zeta, S_{f0}, S_{nx0}]^T$ denote the vector of modal parameters to be identified.

Consider the discrete estimator of the spectral density $S_x(\omega)$ of the stochastic process $x(t)$:

$$S_{x,N}(\omega_k) = \frac{\Delta t}{2\pi N}\left|\sum_{m=0}^{N-1} x(m)\exp(-i\omega_k m\Delta t)\right|^2 \tag{6}$$

where $\omega_k = k\Delta\omega$, $k = 0, \ldots, N_1 - 1$ with $N_1 = \mathrm{INT}[N/2]$, $\Delta\omega = 2\pi/T$, and $T = N\Delta t$. Here INT denotes integer part. Similarly, for measured data $\hat{\boldsymbol{X}}_N = [\hat{x}(0), \ldots, \hat{x}(N-1)]^T$ the corresponding estimator of the spectral density of the process $\hat{x}(t)$ has the form

$$S_{\hat{x},N}(\omega_k) = \frac{\Delta t}{2\pi N}\left|\sum_{m=0}^{N-1} \hat{x}(m)\exp(-i\omega_k m\Delta t)\right|^2 \tag{7}$$

The estimator $S_{\hat{x},N}(\omega_k)$ is asymptotically unbiased; that is,

$$\lim_{N\to\infty} E[S_{\hat{x},N}(\omega_k)] = S_x(\omega_k) + S_{nx0} \tag{8}$$

where $E[\,]$ denotes expectation. However, for finite N this estimator is biased, which implies that equality 8 does not hold without taking the limit. Using Eqs. (4) and (7) and taking expectation yields

$$E[S_{\hat{x},N}(\omega_k)] = E[S_{x,N}(\omega_k)] + S_{nx0} = \frac{\Delta t}{2\pi N}\sum_{m,p=0}^{N-1}\exp[i\omega_k(m-p)\Delta t]R_x[(m-p)\Delta t] + S_{nx0} \tag{9}$$

Grouping together terms having the same value of $|m-p|$, we obtain the following expression:

$$E[S_{x,N}(\omega_k)] = \frac{\Delta t}{2\pi N}\sum_{m=0}^{N-1} a_m R_x(m\Delta t)\cos(m\omega_k\Delta t) \tag{10}$$

where

$$a_m = N, \qquad m = 0$$
$$a_m = 2(N-m), \qquad m \geq 1 \tag{11}$$

Note that the right-hand side of Eq. (10) can be calculated efficiently by using the fast Fourier transform (FFT) of the sequence $a_m R_x(m\Delta t)$, $m = 0, 1, \ldots, N-1$.

The estimator $S_{x,N}(\omega_k)$, given by Eq. (6), can be rewritten in the form

$$S_{x,N}(\omega_k) = \xi_1^2(\omega_k) + \xi_2^2(\omega_k) \tag{12}$$

where

$$\xi_1(\omega_k) = \sqrt{\frac{\Delta t}{2\pi N}}\sum_{m=0}^{N-1} x(m)\cos(\omega_k m\Delta t)$$
$$\xi_2(\omega_k) = \sqrt{\frac{\Delta t}{2\pi N}}\sum_{m=0}^{N-1} x(m)\sin(\omega_k m\Delta t) \tag{13}$$

The process $x(t)$, being the response of the SDOF system governed by Eq. (1), is a Gaussian process with zero mean. Therefore, each of the random variables $\xi_1(\omega_k)$ and $\xi_2(\omega_k)$ is also Gaussian distributed with zero mean. Furthermore, for a fixed Δt, and asymptotically, as $N\to\infty$, the random variables $\xi_1(\omega_k)$ and $\xi_2(\omega_k)$ are independent and have variances each equal to $\frac{1}{2}S_x(\omega_k)$ (Ref. 23). It, therefore, follows that the estimator $S_{x,N}(\omega_k)$ has the following asymptotic behavior:

$$\lim_{N\to\infty} S_{x,N}(\omega_k) = \tfrac{1}{2}S_x(\omega_k)\chi_2 \tag{14}$$

where χ_2 is a random variable having chi-square distribution with two degrees of freedom. The PDF of the random variable $Y(\omega_k) = \lim_{N\to\infty} S_{x,N}(\omega_k)$ is, therefore, given by

$$p[Y(\omega_k)] = \frac{1}{S_x(\omega_k)}\exp\left[-\frac{Y(\omega_k)}{S_x(\omega_k)}\right] \tag{15}$$

In the case of finite N the random variables $\xi_1(\omega_k)$ and $\xi_2(\omega_k)$ are not independent and their variances are not equal. However, it can be verified by using simulations that for $k \ll N_1$ the PDF of $S_{x,N}(\omega_k)$ can be accurately approximated by a chi-square distribution in analogy to Eq. (15) as follows:

$$p[S_{x,N}(\omega_k)] \simeq \frac{1}{E[S_{x,N}(\omega_k)]}\exp\left\{-\frac{S_{x,N}(\omega_k)}{E[S_{x,N}(\omega_k)]}\right\} \tag{16}$$

where $E[S_{x,N}(\omega_k)]$ is given by Eq. (10).

Notice that Eq. (12) is also correct for $S_{\hat{x},N}(\omega_k)$ if we substitute $\hat{x}(m)$ for $x(m)$ in Eq. (13). Therefore, for $k \ll N_1$, the PDF of $S_{\hat{x},N}(\omega_k)$ can also be accurately approximated by a chi-square distribution with two degrees of freedom.

Furthermore, simulations show that the random variables $S_{x,N}(\omega_k)$ and $S_{x,N}(\omega_l)$, with $k \neq l$ and $k, l \ll N_1$, are uncorrelated. According to Ref. 23, uncorrelated chi-square random variables are independent. Therefore, for a sufficiently small number $K < N_1$, one

can assume that the random vector $\boldsymbol{S}_{x,N}^{K} = \{S_{x,N}(0), S_{x,N}(\Delta\omega), \ldots, S_{x,N}[(K-1)\Delta\omega]\}^T$ has all its elements approximately independently chi-square distributed. Therefore, its joint PDF can be approximated as follows:

$$p\left(\boldsymbol{S}_{x,N}^{K}\right) \simeq \prod_{k=0}^{K-1} \frac{1}{E[S_{x,N}(\omega_k)]} \exp\left\{-\frac{S_{x,N}(\omega_k)}{E[S_{x,N}(\omega_k)]}\right\} \tag{17}$$

Given the observed data $\hat{\boldsymbol{X}}_N$, one may calculate by using Eq. (7) the corresponding observed estimate vector $\boldsymbol{S}_{\hat{x},N}^{K} = \{S_{\hat{x},N}(0), S_{\hat{x},N}(\Delta\omega), \ldots, S_{\hat{x},N}[(K-1)\Delta\omega]\}^T$. With the use of Bayes's theorem, the updated PDF of the model parameters $\boldsymbol{a}$ given the data $\boldsymbol{S}_{\hat{x},N}^{K}$ is given by

$$p\left(\boldsymbol{a} \mid S_{\hat{x},N}^{K}\right) = c_1 p(\boldsymbol{a}) p\left(\boldsymbol{S}_{\hat{x},N}^{K} \mid \boldsymbol{a}\right) \tag{18}$$

where c_1 is a normalizing constant, and $p(\boldsymbol{S}_{\hat{x},N}^{K} \mid \boldsymbol{a})$ is given, in analogy to Eq. (17), by

$$p\left(\boldsymbol{S}_{\hat{x},N}^{K} \mid \boldsymbol{a}\right) \simeq \prod_{k=0}^{K-1} \frac{1}{E[S_{\hat{x},N}(\omega_k \mid \boldsymbol{a})]} \exp\left\{-\frac{S_{\hat{x},N}(\omega_k)}{E[S_{\hat{x},N}(\omega_k \mid \boldsymbol{a})]}\right\} \tag{19}$$

where $E[S_{\hat{x},N}(\omega_k \mid \boldsymbol{a})]$ is calculated from Eqs. (9) and (10) with $R_x(m\Delta t) = R_x(m\Delta t \mid \boldsymbol{a})$ calculated from Eq. (2). The most probable parameters $\hat{\boldsymbol{a}}$, referred to as optimal parameters, are obtained by maximizing the posterior PDF in Eq. (18), or equivalently, by minimizing $g(\boldsymbol{a}) = -\ell n[p(\boldsymbol{a})p(\boldsymbol{S}_{\hat{x},N}^{K} \mid \boldsymbol{a})]$. It is verified by using numerical examples that the updated PDF of the parameters $\boldsymbol{a}$ can be well approximated by a Gaussian distribution $N[\hat{\boldsymbol{a}}, \boldsymbol{H}^{-1}(\hat{\boldsymbol{a}})]$ with mean $\hat{\boldsymbol{a}}$ and covariance matrix $\boldsymbol{H}^{-1}(\hat{\boldsymbol{a}})$, where $\boldsymbol{H}(\hat{\boldsymbol{a}})$ denotes the Hessian of $g(\boldsymbol{a})$ calculated at $\boldsymbol{a} = \hat{\boldsymbol{a}}$.

In the case in which several independent time histories $\hat{\boldsymbol{X}}_N^{(1)}, \ldots, \hat{\boldsymbol{X}}_N^{(M)}$ are available, the estimation can proceed by calculating the corresponding estimates $\boldsymbol{S}_{\hat{x},N}^{K,(1)}, \ldots, \boldsymbol{S}_{\hat{x},N}^{K,(M)}$ and then the updated PDF:

$$p\left(\boldsymbol{a} \mid \boldsymbol{S}_{\hat{x},N}^{K,(1)}, \ldots, \boldsymbol{S}_{\hat{x},N}^{K,(M)}\right) = c_2 p(\boldsymbol{a}) \prod_{m=1}^{M} p\left(\boldsymbol{S}_{\hat{x},N}^{K,(m)} \mid \boldsymbol{a}\right) \tag{20}$$

where each of the terms in this product is calculated by using Eq. (19). As before, one can approximate the posterior PDF with a Gaussian distribution centered at the optimal parameters $\hat{\boldsymbol{a}}$ obtained by maximizing the right-hand side of Eq. (20).

An alternative approach, which yields equivalent results but can be shown to be computationally more efficient, is to calculate the average of the above M spectral density estimates and use an equation analogous to Eq. (19) where the right-hand side involves chi-square distributions with $2M$ degrees of freedom. This is because, as discussed in Sec. IV, such an averaged spectral density estimator follows a chi-square distribution with $2M$ degrees of freedom with the same mean value as before; that is, the one given by Eq. (9).

Note that in practice, in the case of multiple sets of data, one of the following two approaches is usually followed: 1) one calculates the average spectrum and then uses curve fitting to obtain the optimal parameters; 2) one first calculates the optimal estimates $\hat{\boldsymbol{a}}^{(1)}, \ldots, \hat{\boldsymbol{a}}^{(M)}$, using curve fitting for each of the M sets of data, and then calculates the overall optimal value $\hat{\boldsymbol{a}}$ and the covariance of $\boldsymbol{a}$ as the mean and covariance of these individual optimal estimates. In the first case, one obtains only the optimal estimates, whereas in the second case, one obtains also an estimate of the associated uncertainties. However, it is worth noting that the traditionally used least-squares curve fitting of the spectrum estimate $S_{\hat{x},N}(\omega_k)$ is not appropriate. Least squares would be appropriate for calculating the optimal parameters only if the joint distribution of the spectral estimates was a product of Gaussian distributions with the same variance. However, this is not the case, as can be seen from Eq. (19).

Although the preceding formulation was presented for the particular case in which the measured response is assumed to consist of displacement histories, it can be easily modified to treat velocity or acceleration measurements. In this case one must simply use in the right-hand side of Eqs. (2) and (3) the corresponding expressions for velocity or acceleration.

B. MDOF Case

Consider a system with N_d degrees of freedom (DOF) and the equation of motion

$$\boldsymbol{M}\ddot{\boldsymbol{x}} + \boldsymbol{C}\dot{\boldsymbol{x}} + \boldsymbol{K}\boldsymbol{x} = \boldsymbol{F}(t) \tag{21}$$

where $\boldsymbol{M}$, $\boldsymbol{C}$, and $\boldsymbol{K}$ are the mass, damping, and stiffness matrices of the oscillator, respectively, and $\boldsymbol{F}(t)$ is Gaussian white noise with spectral density $\boldsymbol{S}_F(\omega) \equiv \boldsymbol{S}_{F0}$.

Assume that discrete data are available at $N_s (\leq N_d)$ measured DOFs. Also, assume that as a result of measurement noise and modeling error there is a difference between the measured response $\hat{\boldsymbol{x}}(m) \in R^{N_s}$ and the model response $\boldsymbol{x}(m)$ at the measured degrees of freedom, which can be adequately represented by discrete zero-mean Gaussian white noise $\boldsymbol{n}_x(m) \in R^{N_s}$. That is,

$$\hat{\boldsymbol{x}}(m) = \boldsymbol{L}_0 \boldsymbol{x}(m) + \boldsymbol{n}_x(m) \tag{22}$$

where $\boldsymbol{L}_0$ is an $N_s \times N_d$ observation matrix, composed of zeros and ones, and $\boldsymbol{n}_x(m)$ is a white noise process, modeling measurement noise and modeling error, with $N_s \times N_s$ constant spectral density matrix $\boldsymbol{S}_{nx}(\omega) \equiv \boldsymbol{S}_{nx0}$.

Using modal analysis, we obtain the uncoupled modal equations of motion

$$\ddot{q}_r(t) + 2\zeta_r\omega_r\dot{q}_r(t) + \omega_r^2 q_r(t) = f_r(t), \qquad r = 1, \ldots, N_d \tag{23}$$

where $\boldsymbol{q}(t) = [q_1(t), \ldots, q_{N_d}(t)]^T$ are the modal coordinates and $\boldsymbol{f}(t) = [f_1(t), \ldots, f_{N_d}(t)]^T$ is the modal forcing vector. The transformation between the original coordinates (forces) and the modal coordinates (forces) is given by $\boldsymbol{x}(t) = \boldsymbol{\Phi} \cdot \boldsymbol{q}(t)$ and $\boldsymbol{f}(t) = (\boldsymbol{M}\boldsymbol{\Phi})^{-1} \cdot \boldsymbol{F}(t)$.

Here $\boldsymbol{\Phi}$ denotes the modeshape matrix, composed of the modeshape vectors $\boldsymbol{\phi}^{(r)}$ which are assumed to be normalized so that $\phi_{i_r}^{(r)} = 1$, $r = 1, \ldots, N_d$, where i_r is a measured DOF that is not a node of the rth mode.

The spectral density matrix of the modal forcing vector $\boldsymbol{f}(t)$ is given by

$$\boldsymbol{S}_f(\omega) = \boldsymbol{S}_{f0} = (\boldsymbol{M}\boldsymbol{\Phi})^{-1}\boldsymbol{S}_{F0}(\boldsymbol{M}\boldsymbol{\Phi})^{-T} \tag{24}$$

Here, we will assume that only N_m modes contribute significantly to the response and we will identify only the modal parameters corresponding to these modes. Specifically, the parameter vector $\boldsymbol{a}$ for identification is composed of 1) the parameters $\omega_r, \zeta_r, r = 1, \ldots, N_m$; 2) the elements of the first N_m columns of the $N_s \times N_d$ matrix $\boldsymbol{L}_0\boldsymbol{\Phi}$, except those elements that were used for the normalization of the modeshapes that are assumed constant and equal to one; thus, a total of $N_m(N_s - 1)$ unknown modeshape parameters are to be identified; 3) the elements of the upper left $N_m \times N_m$ part of the modal forcing spectral density matrix $\boldsymbol{S}_{f0}$; and 4) all elements of the $N_s \times N_s$ matrix $\boldsymbol{S}_{nx0}$. It is known[22] that the response $\boldsymbol{x}(t)$ for given parameters $\boldsymbol{a}$ is a Gaussian process with zero mean and spectral density:

$$S_x^{(j,l)}(\omega \mid \boldsymbol{a}) \simeq \sum_{r=1}^{N_m}\sum_{s=1}^{N_m} \phi_j^{(r)}\phi_l^{(s)} \times \frac{S_{f0}^{(r,s)}}{\left[\left(\omega_r^2 - \omega^2\right) + 2i\omega\omega_r\zeta_r\right]\left[\left(\omega_s^2 - \omega^2\right) - 2i\omega\omega_s\zeta_s\right]} \tag{25}$$

Recall that here the scaling of each modeshape is chosen such that one of its components corresponding to a measured DOF is equal to unity. However, such scaling is arbitrary, and the above vectors can be identified only up to a constant scaling factor. A different modeshape normalization will cause all observed components of the rth modeshape to be scaled by some constant c_r; at the same time the values of the elements $S_{f0}^{(r,s)}$ of the modal forcing spectral density matrix will be scaled by $(c_r c_s)^{-1}$.

Consider the stochastic vector process $\boldsymbol{x}(t)$ and the discrete estimator of its spectral density matrix $\boldsymbol{S}_x(\omega)$ with (j,l) element:

$$S_{x,N}^{(j,l)}(\omega_k) = \frac{\Delta t}{2\pi N} \sum_{m,p=0}^{N-1} x_j(m) x_l(p) \exp[-i\omega_k (p-m)\Delta t] \quad (26)$$

where $\omega_k = k\Delta\omega$, $k = 0, \ldots, N_1 - 1$ with $N_1 = \text{INT}[N/2]$, $\Delta\omega = 2\pi/T$, and $T = N\Delta t$. Similarly, for measured data $\hat{\boldsymbol{X}}_N = \{\hat{\boldsymbol{x}}(m), m = 1, \ldots, N\}$ the corresponding estimator of the spectral density matrix of the random vector process $\hat{\boldsymbol{x}}(t)$ has the form

$$S_{\hat{x},N}^{(j,l)}(\omega_k) = \frac{\Delta t}{2\pi N} \sum_{m,p=0}^{N-1} \hat{x}_j(m) \hat{x}_l(p) \exp[-i\omega_k (p-m)\Delta t] \quad (27)$$

This estimator $\boldsymbol{S}_{\hat{x},N}(\omega_k)$ is asymptotically unbiased; that is,

$$\lim_{N\to\infty} E[\boldsymbol{S}_{\hat{x},N}(\omega_k)] = \boldsymbol{L}_0 \boldsymbol{S}_x(\omega_k) \boldsymbol{L}_0^T + \boldsymbol{S}_{nx0} \quad (28)$$

where $E[\,]$ denotes expectation. However, for finite N this estimator is biased, which implies that equality (28) does not hold without taking the limit.

Calculation of the expectation of this estimator for finite N yields

$$\begin{aligned} E[\boldsymbol{S}_{\hat{x},N}(\omega_k) \mid \boldsymbol{a}] &= \boldsymbol{L}_0 E[\boldsymbol{S}_{x,N}(\omega_k) \mid \boldsymbol{a}] \boldsymbol{L}_0^T + \boldsymbol{S}_{nx0} \\ &= (\boldsymbol{L}_0 \boldsymbol{\Phi}) E[\boldsymbol{S}_{q,N}(\omega_k) \mid \boldsymbol{a}] (\boldsymbol{L}_0 \boldsymbol{\Phi})^T + \boldsymbol{S}_{nx0} \end{aligned} \quad (29)$$

where $E[S_{q,N}^{(r,s)}(\omega_k)]$ can be calculated by using FFT, from an expression analogous to Eq. (10), as follows:

$$\begin{aligned} E\big[S_{q,N}^{(r,s)}(\omega_k)\big] = \frac{\Delta t}{4\pi N} \sum_{m=0}^{N-1} a_m \big[& R_q^{(r,s)}(m\Delta t) \\ & + R_q^{(s,r)}(m\Delta t)\big] \exp(-i\omega_k m \Delta t) \end{aligned} \quad (30)$$

where the coefficients a_m, $m = 0, \ldots, N-1$ are given by Eq. (11).

Here, the correlation functions $R_q^{(r,s)}(t)$ are given by

$$R_q^{(r,s)}(t) = R_{f0}^{(r,s)} \int_0^\infty h_r(t+\tau) h_s(\tau)\, \mathrm{d}\tau, \qquad t > 0 \quad (31)$$

where $h_r(t)$ is the impulse response function for the rth mode corresponding to the quantity of interest (e.g., displacement, velocity, or acceleration).

Assume now a set of independent time histories $\boldsymbol{X}_N^{(1)}, \ldots, \boldsymbol{X}_N^{(M)}$ and let $\boldsymbol{S}_{x,N}^{(1)}, \ldots, \boldsymbol{S}_{x,N}^{(M)}$ denote the corresponding spectral matrix estimates. It can be shown[24] that the matrix

$$\boldsymbol{S}_{x,N}^M(\omega_k) = \frac{1}{M} \sum_{m=1}^M \boldsymbol{S}_{x,N}^{(m)}(\omega_k)$$

in the limit when $N \to \infty$ follows a complex Wishart distribution of dimension N_s with M DOF and mean $\boldsymbol{S}_x(\omega_k)$:

$$p\big[\boldsymbol{S}_{x,N}^M(\omega_k)\big] = c_3 \frac{\big|\boldsymbol{S}_{x,N}^M(\omega_k)\big|^{M-N_s}}{|\boldsymbol{S}_x(\omega_k)|^M} \exp\Big\{-M \operatorname{tr}\big[\boldsymbol{S}_x^{-1}(\omega_k) \boldsymbol{S}_{x,N}^M(\omega_k)\big]\Big\} \quad (32)$$

where c_3 is a normalizing constant. Here $|\boldsymbol{A}|$ and $\operatorname{tr}[\boldsymbol{A}]$ are used to denote the determinant and trace of a matrix $\boldsymbol{A}$, respectively. It is important to note that this PDF exists only when $M \geq N_s$.

In the special case for which $N_s = 1$ and $M = 1$, this distribution becomes a chi-square distribution with two degrees of freedom. That is, Eq. (32) reduces to Eq. (15). In the case in which $M > 1$, the diagonal elements $[\boldsymbol{Y}^M(\omega_k)]_{i,i}$ are chi-square distributed with $2M$ degrees of freedom and mean $[\boldsymbol{S}_x(\omega_k)]_{i,i}$ (Ref. 25).

It can be shown by using simulations that for finite N and for $k \ll N_1$ the PDF of

$$\boldsymbol{S}_{\hat{x},N}^M(\omega_k) = \frac{1}{M} \sum_{m=1}^M \boldsymbol{S}_{\hat{x},N}^{(m)}(\omega_k)$$

can be accurately approximated in a manner similar to Eq. (32) by a Wishart distribution with mean $E[\boldsymbol{S}_{\hat{x},N}^M(\omega_k)]$ given by Eq. (29). Thus, $p[\boldsymbol{S}_{\hat{x},N}^M(\omega_k)]$ is given by Eq. (32) by replacing x by $\hat{x}$. Furthermore, it can be shown by using simulations that the random matrices $\boldsymbol{S}_{x,N}^M(\omega_k)$ and $\boldsymbol{S}_{x,N}^M(\omega_l)$ with $k \neq l$ and $k, l \ll N_1$ are uncorrelated and, therefore, independent.[23] Thus, for a sufficiently small number $K < N_1$, one can assume that the random tensor $\boldsymbol{S}_{\hat{x},N}^{M,K} = \{\boldsymbol{S}_{\hat{x},N}^M(0), \boldsymbol{S}_{\hat{x},N}^M(\Delta\omega), \ldots, \boldsymbol{S}_{\hat{x},N}^M[(K-1)\Delta\omega]\}^T$ has all its elements approximately independently Wishart distributed. Therefore, its joint PDF can be approximated as follows:

$$\begin{aligned} p\big(\boldsymbol{S}_{\hat{x},N}^{M,K} \,\big|\, \boldsymbol{a}\big) \simeq c_4 \prod_{k=1}^K & \frac{\big|\boldsymbol{S}_{\hat{x},N}^M(\omega_k)\big|^{M-N_s}}{|E[\boldsymbol{S}_{\hat{x},N}(\omega_k) \mid \boldsymbol{a}]|^M} \\ & \times \exp\Big(-M \operatorname{tr}\big\{E[\boldsymbol{S}_{\hat{x},N}(\omega_k) \mid \boldsymbol{a}]^{-1} \boldsymbol{S}_{\hat{x},N}^M(\omega_k)\big\}\Big) \end{aligned} \quad (33)$$

where c_4 is a normalizing constant and $E[\boldsymbol{S}_{\hat{x},N}(\omega_k) \mid \boldsymbol{a}]$ is calculated from Eqs. (29) and (30) with $\boldsymbol{R}_q(m\Delta t) = \boldsymbol{R}_q(m\Delta t \mid \boldsymbol{a})$ calculated from Eq. (31).

The proposed approach can be summarized as follows. Given $M \geq N_s$ independent sets of observed data $\hat{\boldsymbol{X}}_N^{(m)}$, $m = 1, \ldots, M$, one may calculate the corresponding observed matrix estimates $\boldsymbol{S}_{\hat{x},N}^{(m)}$, $m = 1, \ldots, M$ by using Eq. (27). Next, one can calculate

$$\boldsymbol{S}_{\hat{x},N}^M(\omega_k) = \frac{1}{M} \sum_{m=1}^M \boldsymbol{S}_{\hat{x},N}^{(m)}(\omega_k)$$

and then the random tensor $\boldsymbol{S}_{\hat{x},N}^{M,K} = \{\boldsymbol{S}_{\hat{x},N}^M(0), \boldsymbol{S}_{\hat{x},N}^M(\Delta\omega), \ldots, \boldsymbol{S}_{\hat{x},N}^M[(K-1)\Delta\omega]\}^T$. With the use of Bayes's theorem, the updated PDF of the model parameters $\boldsymbol{a}$ given the data $\boldsymbol{S}_{\hat{x},N}^{M,K}$ is then given by

$$p\big(\boldsymbol{a} \,\big|\, \boldsymbol{S}_{\hat{x},N}^{M,K}\big) = c_5\, p(\boldsymbol{a})\, p\big(\boldsymbol{S}_{\hat{x},N}^{M,K} \,\big|\, \boldsymbol{a}\big) \quad (34)$$

where c_5 is a normalizing constant, and $p(\boldsymbol{S}_{\hat{x},N}^{M,K} \mid \boldsymbol{a})$ is given by Eq. (33). The most probable parameters $\hat{\boldsymbol{a}}$ are obtained by minimizing $g(\boldsymbol{a}) = -\ell n[p(\boldsymbol{a})\, p(\boldsymbol{S}_{\hat{x},N}^{M,K} \mid \boldsymbol{a})]$. Furthermore, as in the SDOF case, it is found that the updated PDF of the parameters $\boldsymbol{a}$ can be well approximated by a Gaussian distribution $N[\hat{\boldsymbol{a}}, \boldsymbol{H}^{-1}(\hat{\boldsymbol{a}})]$ with mean $\hat{\boldsymbol{a}}$ and covariance matrix $\boldsymbol{H}^{-1}(\hat{\boldsymbol{a}})$, where $\boldsymbol{H}(\hat{\boldsymbol{a}})$ denotes the Hessian of $g(\boldsymbol{a})$ calculated at $\boldsymbol{a} = \hat{\boldsymbol{a}}$.

Note that the proposed approach can be also applied in the case of non-Gaussian input/response because the FFTs remain Gaussian.[26] Efforts are currently underway to extend the methodology for the case of nonwhite input.[27]

III. Numerical Examples

A. Example 1: SDOF System

In this example, we consider a SDOF system and we study the statistical properties of the estimator $S_{x,N}(\omega_k)$. The simulated response histories $\hat{\boldsymbol{X}}_N$ are generated for a SDOF oscillator with parameters $\tilde{\boldsymbol{a}} = [\tilde{\omega}_0, \tilde{\zeta}, \tilde{S}_{f0}]^T$, where $\tilde{\omega}_0 = 3$ rad/s, $\tilde{\zeta} = 2\%$, and $\tilde{S}_{f0} = 5N^2$ s. The time step at which the data are sampled is assumed to be $\Delta t = 0.05$ s, with a total time interval $T = 1000$ s, that is, $N = 20{,}000$. However, in order to simulate reality and the presence of aliasing, the simulation of excitation history and the integration of the equation of motion was performed by using a much smaller step of $\Delta t/10$. The response measurements are assumed to be noise free in this example; that is, $\tilde{S}_{nx0} = 0$.

In examples 1 and 2 the MATLAB® subroutine lsim was used to integrate the equation of motion. Furthermore, noninformative prior distributions were assumed in both examples. That is, only the dynamic data are assumed to contribute to the posterior PDF.

Figure 1 shows a comparison among $S_x(\omega \mid \tilde{\boldsymbol{a}})$ (solid curve), $E[S_{x,N}(\omega_k \mid \tilde{\boldsymbol{a}})]$ calculated from Eq. (10) (dashed curve), and $E[S_{x,N}(\omega_k \mid \tilde{\boldsymbol{a}})]$ calculated by using 2000 simulations (dotted curve). The second and third curves are indistinguishable, implying that Eq. (10) is accurate. Observing the relative difference between the first two curves, one can conclude that the error made if $E[S_{x,N}(\omega_k) \mid \tilde{\boldsymbol{a}}]$ is assumed to be equal to $S_x(\omega \mid \tilde{\boldsymbol{a}})$ is large, especially as one moves to higher frequencies. The reason for this observed difference is aliasing. In addition, detailed observation reveals that at frequencies around the natural frequency, the values

Table 1 Identification results for one set of data (example 1)

Parameter	Actual $\tilde{a}$	Optimal $\hat{a}$	SD σ	COV α	$\beta = (\lvert\tilde{a} - \hat{a}\rvert)/\sigma$
ω_0	3.0000	2.9894	0.0085	0.0028	1.2471
ζ	0.0200	0.0213	0.0028	0.1400	0.4643
S_{f0}	5.0000	5.1134	0.2369	0.0474	0.4787

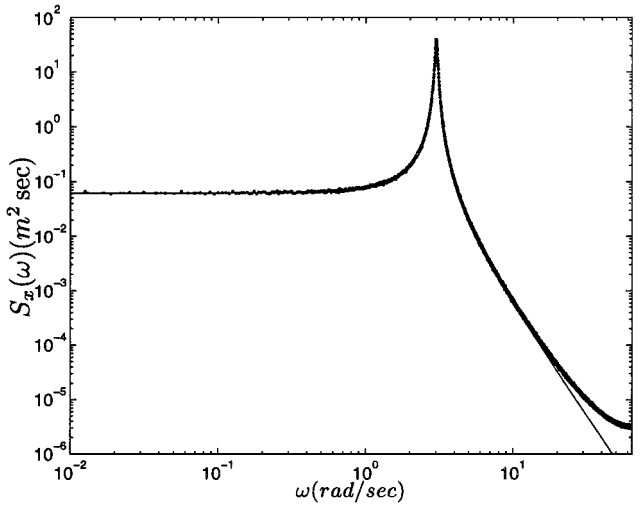

Fig. 1 Comparison among ——, $S_x(\omega)$; - - -, $E[S_{x,N}(\omega)]$ from Eq. (10); and . . . , $E[S_{x,N}(\omega)]$ calculated from 2000 simulations.

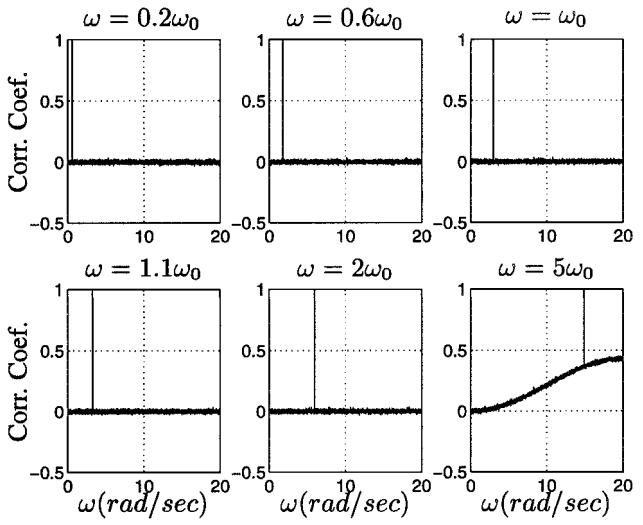

Fig. 2 Coefficients of correlation between $S_{x,N}(\omega_k)$ and $S_{x,N}(\omega_l)$ over the range of ω_l for six values of ω_k.

of the estimator are smaller than the corresponding values of the theoretical spectral density as a result of leakage.

Figure 2 shows the coefficients of correlation between $S_{x,N}(\omega_k)$ and $S_{x,N}(\omega_l)$, $l = 0, \ldots, N_1 - 1$ for various values of ω_k. It can be seen that one can consider the values of $S_{x,N}(\omega_k)$ in the lower frequency range (e.g., for $\omega < 1.5\tilde{\omega}_0$) to be uncorrelated, thus validating the use of Eq. (17). Furthermore, comparison between the cumulative distribution function (CDF) of $S_{x,N}(\omega_k)$ obtained 1) using data from the same 2000 simulations used in Fig. 1 (solid curve) and 2) assuming a chi-square distribution according to Eq. (16) (dashed curve) reveals that the chi-square distribution provides a very good approximation over this range of frequencies. Such plots are not included here because of space limitations.

Table 1 shows the estimated optimal values $\hat{\boldsymbol{a}} = [\hat{\omega}_0, \hat{\zeta}, \hat{S}_{f0}]^T$ and the calculated standard deviations σ_{ω_0}, σ_ζ, and $\sigma_{S_{f0}}$, the coefficient of variation (COV) for each parameter, and the absolute values of the differences between the identified optimal and actual values, normalized with respect to the corresponding standard deviations,

Table 2 Statistics of identification results from 100 simulations (example 1)

Parameter	Actual	Average (optimal)	SD (optimal)	Average (SD)
ω_0	3.0000	3.0002	0.0082	0.0084
ζ	0.0200	0.0205	0.0031	0.0028
S_{f0}	5.0000	4.9960	0.2471	0.2310

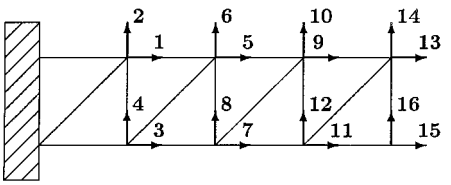

Fig. 3 Four-bay truss (example 2).

obtained by using only one set of data $\hat{\boldsymbol{X}}_N$. Here the updating of the modal parameters was performed by using only spectral estimates up to frequency $\omega_{K-1} = 1.2\tilde{\omega}_0$ [$K = 580$ in Eq. (17)] to ensure that the spectral estimates at different frequencies are uncorrelated to one another. Note that the optimal parameters $\tilde{\boldsymbol{a}}$ were obtained by minimizing the function $g(\boldsymbol{a})$, using the MATLAB subroutine constr. The covariance matrix was calculated as the inverse of the Hessian of $g(\tilde{\boldsymbol{a}})$, the latter being obtained by using finite differences.

Plotting the conditional PDF of various parameters (keeping all other parameters fixed at their optimal values) calculated from Eq. (18) against the Gaussian approximation $N[\hat{\boldsymbol{a}}, \boldsymbol{H}^{-1}(\hat{\boldsymbol{a}})]$ reveals that the latter Gaussian approximation is very accurate. Such plots are not included here because of space limitations.

Next, 100 independent time-history samples were generated, using the same parameters as discussed in the beginning of this example. The optimal parameters $\hat{\boldsymbol{a}}^{(m)}$, $m = 1, \ldots, 100$ were calculated, using each set of data separately. Then, the mean value and the standard deviations of the optimal parameters were calculated from the set $\{\hat{\boldsymbol{a}}^{(m)}, m = 1, \ldots, 100\}$ and are shown in the third and fourth columns, respectively, of Table 2. The last column in this table shows the mean value of the 100 different standard deviations obtained by considering each of these sets of data separately. It can be seen that the last two columns look similar, implying that the uncertainties calculated from a single sample are representative of the uncertainties of the optimal parameters obtained from several independent sets of data of equal length.

B. Example 2: Four-Bay Truss

The second example refers to the truss shown in Fig. 3, where it is assumed that the accelerations at the 8th, 12th, and 15th DOFs were measured over a time interval $T_0 = 4$ s, using a sampling interval $\Delta t = 1/5000$ s. As in example 1, a step of $\Delta t/10$ was used in the integration of the equation of motion, using lsim. The structure is assumed to be excited at all 16 DOFs with independent band-limited Gaussian white noise. The length of all the horizontal and vertical members is equal to 0.5 m. All members have the same cross sectional area $A = 0.0004\ \text{m}^2$. The mass density is $\rho = 7860\ \text{kg/m}^3$, and the modulus of elasticity is $E = 200$ GPa. The first four natural frequencies are 548.4232, 1880.096, 2706.7155 and 3611.284 rad/s, respectively. The damping ratio is assumed to be 2% for all modes. The spectral intensities of the excitation are assumed to be $100N^2$ s for all DOFs. The measurement noise and modeling error levels are assumed to be 10%; that is, the rms of the noise for a particular channel of measurement is equal to 10% of the rms of the noise-free response at the corresponding DOF. Identification using the proposed approach is carried out for the following four cases:

Case 1: Only response measurements from the eighth DOF are used to identify the lowest two modes, utilizing only the spectral estimates up to frequency $\omega_{K-1} = 2124$ rad/s ($K = 677$).

Case 2: Only response measurements from the 12th DOF are used to identify the lowest two modes, utilizing the same range of frequencies as in case 1.

Case 3: Response measurements from the 8th and 15th DOFs are used to identify the lowest two modes, utilizing the same range of frequencies as in case 1.

Table 3 Identification results for case 1 (example 2)

Parameter	Actual $\tilde{a}$	Optimal $\hat{a}$	SD σ	COV α	$\beta = (\lvert\tilde{a} - \hat{a}\rvert)/\sigma$
ω_1	548.4232	548.6063	2.1397	0.0039	0.0856
ω_2	1880.096	1881.0424	3.5494	0.0019	0.2666
ζ_1	0.0200	0.0265	0.0040	0.2024	1.5984
ζ_2	0.0200	0.0190	0.0020	0.0997	0.4819
$S_{f0}^{(1,1)}$	0.7270	0.7246	0.0612	0.0842	0.0392
$\gamma_{f0}^{(1,2)}$	−0.1702	−0.3428	0.1283	0.7536	1.3460
$S_{f0}^{(2,2)}$	1.8126	1.7695	0.1224	0.0675	0.3526
$S_{na0}^{(1)}$	1.1959	1.126	0.0746	0.0624	0.9363

Table 4 Identification results for case 2 (example 2)

Parameter	Actual $\tilde{a}$	Optimal $\hat{a}$	SD σ	COV α	$\beta = (\lvert\tilde{a} - \hat{a}\rvert)/\sigma$
ω_1	548.4232	549.9078	2.0768	0.0038	0.7148
ω_2	1880.096	1882.6923	7.7934	0.0041	0.3331
ζ_1	0.0200	0.0268	0.0038	0.1902	1.7917
ζ_2	0.0200	0.0250	0.0046	0.2319	1.0860
$S_{f0}^{(1,1)}$	2.0428	2.0546	0.1202	0.0589	0.0983
$\gamma_{f0}^{(1,2)}$	−0.1702	−0.1970	0.1063	0.6246	0.2522
$S_{f0}^{(2,2)}$	0.0391	0.0620	0.0140	0.3576	1.6439
$S_{na0}^{(1)}$	1.2449	1.4902	0.1063	0.0854	2.3081

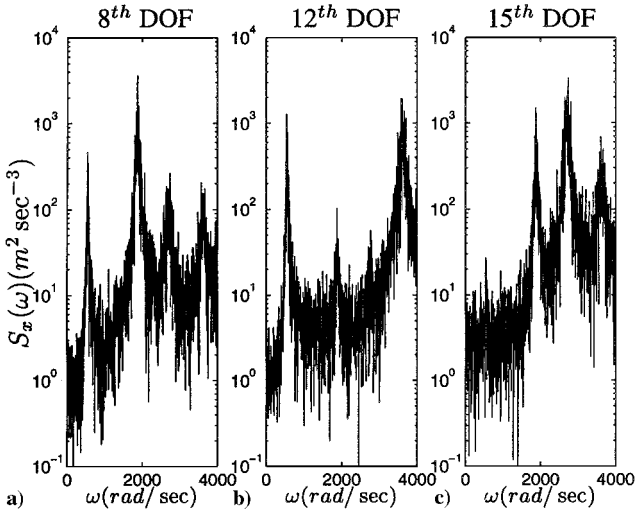

Fig. 4 Acceleration spectral densities for the a) 8th, b) 12th, and c) 15th DOF (example 2).

Case 4: Response measurements from the 8th and 15th DOFs are used to identify the lowest four modes, utilizing only the spectral estimates up to frequency $\omega_{K-1} = 3933$ rad/s ($K = 1253$).

In each of these four cases, two sets ($M = 2$) of response histories are considered, each having length $T = T_0/2 = 2$ s, corresponding to the first and second half of the assumed total response. The reason for this is that our approach requires the number of available data sets to be larger or equal to the number of measured DOFs ($M \geq N_s$). Thus, whereas in cases 1 and 2 one could consider the entire data of length T_0 as one set, in cases 3 and 4 one needs to consider at least two sets.

Figures 4a, 4b, and 4c show the average autospectral densities, corresponding to the 8th, 12th, and 15th DOFs, respectively, obtained from the aforementioned two sets of data. One can see that the relative strength of various modes differs from one DOF to another. Therefore, one expects that the accuracy and uncertainty of the identification results obtained with measurements from different DOFs will vary.

Tables 3–6 show the identification results for cases 1–4, respectively. The interpretation of each column in these tables is the same as that in Table 6. The various groups of rows in each table correspond in the order they appear: modal frequencies, modal damping ratios, modeshape components (for cases, 3 and 4 only), elements of the modal forcing spectral matrix $\boldsymbol{S}_{f0}$, and elements of the noise spectral matrix $\boldsymbol{S}_{na0}$. (Here we use the notation $\boldsymbol{S}_{na0}$ instead of $\boldsymbol{S}_{nx0}$ because the considered measurements are accelerations instead of displacements.) Here, the off-diagonal elements of the matrices $\boldsymbol{S}_{f0}$ and $\boldsymbol{S}_{na0}$ are presented in the form of coherence parameters $\gamma^{(i,j)} \equiv S^{(i,j)}/\sqrt{(S^{(i,i)}S^{(j,j)})}$. Note that in cases 1, 3, and 4, the modeshapes are normalized so that the modeshape component at the 8th DOF is equal to one for each of the modes considered. In contrast, the normalization of the modeshapes in case 2 was done with respect to the 12th DOF. Therefore, direct comparison of the values of the elements of $\boldsymbol{S}_{f0}$ for case 2 and the corresponding values for any of the other three cases is meaningless.

Table 5 Identification results for case 3 (example 2)

Parameter	Actual $\tilde{a}$	Optimal $\hat{a}$	SD σ	COV α	$\beta = (\lvert\tilde{a} - \hat{a}\rvert)/\sigma$
ω_1	548.4232	548.7555	2.2867	0.0042	0.1453
ω_2	1880.096	1879.331	3.3653	0.0018	0.2273
ζ_1	0.0200	0.0302	0.0045	0.2232	2.2826
ζ_2	0.0200	0.0191	0.0019	0.0971	0.4703
$\phi_{15}^{(1)}$	0.1976	0.1973	0.0189	0.0957	0.0180
$\phi_{15}^{(2)}$	−0.6276	−0.6293	0.0065	0.0104	0.2588
$S_{f0}^{(1,1)}$	0.7270	0.8344	0.0744	0.1023	1.4431
$\gamma_{f0}^{(1,2)}$	−0.1702	−0.1659	0.0720	0.4230	0.0604
$S_{f0}^{(2,2)}$	1.8126	1.7792	0.1113	0.0614	0.3002
$S_{na0}^{(1)}$	1.1959	1.2222	0.0904	0.0756	0.2909
$\gamma_{na0}^{(1,2)}$	0	0.1403	0.0369	Inf	3.8008
$S_{na0}^{(2)}$	3.8451	5.0608	0.1591	0.0414	7.6425

Table 6 Identification results for case 4 (example 2)

Parameter	Actual $\tilde{a}$	Optimal $\hat{a}$	SD σ	COV α	$\beta = (\lvert\tilde{a} - \hat{a}\rvert)/\sigma$
ω_1	548.4232	548.8219	2.2902	0.0042	0.1741
ω_2	1880.096	1878.3498	3.3944	0.0018	0.5144
ω_3	2706.7155	2704.2278	4.7330	0.0017	0.5256
ω_4	3611.284	3610.7916	8.7040	0.0024	0.0566
ζ_1	0.0200	0.0304	0.0044	0.2207	2.3653
ζ_2	0.0200	0.0196	0.0018	0.091	0.2398
ζ_3	0.0200	0.0248	0.0018	0.0921	2.5857
ζ_4	0.0200	0.0245	0.0024	0.1193	1.8849
$\phi_{15}^{(1)}$	0.1976	0.2018	0.0173	0.0875	0.2402
$\phi_{15}^{(2)}$	−0.6276	−0.6265	0.0075	0.0120	0.1518
$\phi_{15}^{(3)}$	3.5313	3.4865	0.0795	0.0225	0.5636
$\phi_{15}^{(4)}$	−1.9745	−1.8146	0.0699	0.0354	2.2891
$S_{f0}^{(1,1)}$	0.7270	0.8453	0.0708	0.0974	1.6699
$\gamma_{f0}^{(1,2)}$	−0.1702	−0.0145	0.1429	0.8394	1.0897
$\gamma_{f0}^{(1,3)}$	0.0303	0.0303	0.1881	6.2173	0.0004
$\gamma_{f0}^{(1,4)}$	−0.1339	−0.8413	1.394	10.4095	0.5075
$S_{f0}^{(2,2)}$	1.8126	1.8208	0.0822	0.0454	0.0995
$\gamma_{f0}^{(2,3)}$	0.0247	−0.0618	0.1094	4.4297	0.7907
$\gamma_{f0}^{(2,4)}$	0.1249	0.3549	0.5657	4.5303	0.4066
$S_{f0}^{(3,3)}$	0.1785	0.2597	0.0153	0.0856	5.3184
$\gamma_{f0}^{(3,4)}$	0.0120	−0.1674	0.2329	19.3952	0.7704
$S_{f0}^{(4,4)}$	0.1119	0.1457	0.0163	0.1453	2.0797
$S_{na0}^{(1)}$	1.1959	1.1691	0.0846	0.0707	0.3159
$\gamma_{na0}^{(1,2)}$	0	0.0057	0.0417	Inf	0.1375
$S_{na0}^{(2)}$	3.8451	4.1018	0.1469	0.0382	1.7473

The calculated uncertainties shown in the tables are in accordance with our expectations. For example, the standard deviation of ω_2 in case 2 is more than twice its value in case 1, which is not surprising if one observes that the second mode does not show up as strongly at the 12th DOF (case 2) as it does at the 8th DOF (case 1). Also, as can be seen from Fig. 4, the second mode in the 8th DOF is

more pronounced than the first one (this also can be seen from the fact that in this case the spectral intensity of the first modal force is smaller than that of the second mode; i.e., $S_{f0}^{(1,1)} < S_{f0}^{(2,2)}$). This explains the fact that in case 1, the COVs corresponding to ω_1 and ζ_1 are larger than the corresponding values for ω_2 and ζ_2. Note that the opposite is true in case 2, as the second mode in the 12th DOF is not as strong ($S_{f0}^{(1,1)} > S_{f0}^{(2,2)}$).

A result observed, but not tabulated because of space limitations, is that the calculated standard deviations of the optimal parameters, especially those corresponding to the modeshape components and the spectral intensities, increase rapidly as the noise level increases, which is according to expectations.

It is worth noting that in all cases the COVs for the frequencies are smaller than those of the damping ratios, indicating that frequencies are identified better than dampings. An additional result observed, but not tabulated, is that the modal damping ratios were found to exhibit a significant correlation with the corresponding modal forcing spectral intensities.

Another observation is that the use of additional channels does not necessarily improve the identification results; that is, it does not necessarily reduce the uncertainties of the identified modal parameters. For example, comparing the tabulated results for cases 1 and 3, one sees that the uncertainties is in the modal frequencies and dampings of the first two modes for these two cases are similar. Thus, the additional channel at the 15th DOF provides only information regarding the modeshapes components at the 15th DOF (normalized with respect to the corresponding values at the 8th DOF, which here are assumed to be equal to one). However, it is likely that placement of the second sensor at a different DOF can reduce the uncertainties of the frequencies and/or damping ratios. Rational procedures for selecting the optimal number of sensors and their optimal locations have been developed.[28,29] They are based on a statistical approach for modal updating and involve the minimization of the information entropy, which is a unique measure of the uncertainty of the modal parameters.

Comparing Table 5 (case 3) and Table 6 (case 4), one sees that the consideration of the higher (third and fourth) modes does not have any substantial impact on the values of the optimal parameters and the standard deviations of the two lower modes. However, it can be observed that the identified values for the spectral intensities of the noise are always larger than the theoretical values. The reason for this is that although all 16 modes contribute to the structural response, the identification has been restricted to a small number of the lower modes. The contribution of the higher modes on the lower frequency range has the effect of an equivalent artificial measurement noise, which causes the identified mean values of the noise spectral intensities to be larger than the actual values used in the simulations. As we consider more modes, these errors become smaller, and the estimates of the noise spectral intensities approach the theoretical values. The improvement on the values of the noise spectral density matrix as more modes are considered can be seen by comparing Tables 5 and 6. In Table 5 some of the identified elements of the noise spectral density matrix are far from the corresponding actual values. Furthermore, the estimated uncertainties are unreasonably small as the values of β in the last column are too large. However, as more modes are considered (case 4), this phenomenon starts correcting itself.

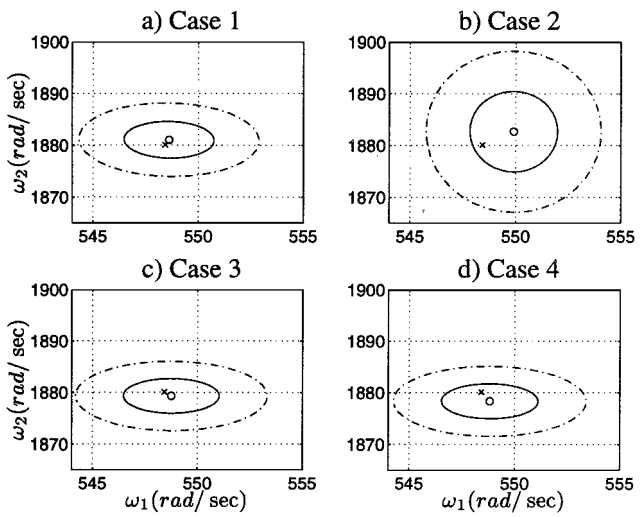

Fig. 5 Optimal point (○), actual point (×), one SD (——), two SDs (– – –), and conditional updated joint PDF of natural frequencies ω_1 and ω_2 for cases 1–4 (example 2).

Figures 5a–5d, corresponding to cases 1–4, respectively, show the contours in the (ω_1, ω_2) plane of the calculated conditional updated PDF of ω_1 and ω_2 obtained from Eq. (34), keeping all other parameters fixed at their optimal values. One observes that in all cases the actual parameters are at a reasonable distance, measured in terms of the estimated standard deviations (SDs), from the identified optimal parameters, which confirms that the calculated uncertainties are reasonable.

IV. Conclusions

A Bayesian spectral density approach for updating the PDF of the modal parameters of a MDOF oscillator using ambient data was presented. The obtained posterior PDF for the modal parameters can be accurately approximated by a multivariate Gaussian distribution. The calculated mean and covariance matrix of this distribution offer an estimate of the optimal (most probable) values of the modal parameters and the associated uncertainties. The quantification of these uncertainties is very important when one plans to use modal estimates for further processing, such as for updating the theoretical finite-element model of a structure. It can be shown that in this case the calculated uncertainties provide a rational basis for weighing differently the errors of the various modal parameters, the errors being the differences between the theoretical and identified values of these parameters.

The presented methodology processes simultaneously the response histories at all measured DOFs. A number of independent sets of response histories are needed. This number can be as small as the number of measured DOFs. For example, in the case of a single measured DOF, one set of data is sufficient for the identification of the modal parameters and their uncertainties. The approach directly uses the corresponding very erratic spectrum without the need for smoothing or averaging. The estimation of the uncertainties does not require calculation of different optimal values, obtained from different data sets, followed by calculation of the statistics of these optimal estimates.

Acknowledgments

Financial support for this research from the Hong Kong Research Grant Council under Grants HKUST 639/95E and HKUST 6041/97E is gratefully acknowledged.

References

[1]Natke, H. G., and Yao, Y. P. T., *Proceedings of the Workshop on Structural Safety Evaluation Based on System Identification Approaches*, Vieweg, Wiesbaden, Germany, 1988.

[2]Berman, A., and Flannelly, W. G., "Theory of Incomplete Models of Dynamics Structures," *AIAA Journal*, Vol. 9, No. 8, 1971, pp. 1481–1487.

[3]Chen, J. C., Peretti, L. F., and Garba, J. A., "Spacecraft Structural System Identification by Modal Test," *Journal of Spacecraft and Rockets*, Vol. 24, No. 1, 1987, pp. 90–94.

[4]Flannelly, W. G., and Berman, A., "The State of the Art of System Identification of Vibrating Structures," *Proceedings of the American Society of Mechanical Engineering Winter Annual Meeting*, American Society of Mechanical Engineers, Fairfield, NJ, 1972, pp. 121–132.

[5]Collins, J. D., Hart, G. C., Hasselman, T. K., and Kennedy, B., "Statistical Identification of Structures," *AIAA Journal*, Vol. 12, No. 2, 1974, pp. 185–190.

[6]Eykhoff, P., *System Identification*, Wiley, New York, 1974.

[7]Cooper, J. E., "Comparison of Some Time Domain System Identification Techniques Using Approximate Data Correlations," *International Journal of Analytical and Experimental Modal Analysis*, Vol. 4, 1989, pp. 51–57.

[8]Vandiver, J. K., Dunwoody, A. B., Campbell, R. B., and Cook, M. F., "A Mathematical Basis for the Random Decrement Vibration Signature Analysis Technique," *Journal of Mechanical Design*, Vol. 104, 1982, pp. 307–313.

[9]Beck, J. L., Vanik, M. W., Polidori, D. C., and May, B. S., "Ambient Vibration Surveys of a Steel Frame Building in a Healthy and Damaged State," Earthquake Engineering Research Lab., TR EERL 97-03, California Inst. of Technology, Pasadena, CA, 1997.

[10]Conte, J. P., and Kumar, S., "Statistical System Identification of Structures Using ARMA Models," in *Proceedings of the 7th American Society of Civil Engineering Specialty Conference on Probabilistic Mechanics and Structural Reliability*, American Society of Civil Engineers, Reston, VA, 1996, pp. 142–145.

[11]Goodwin, G. C., and Sin, K. S., *Adaptive Filtering Prediction and Control*, Prentice–Hall, Upper Saddle River, NJ, 1984.

[12]Kalman, R. E., and Bucy, R. S., "New Results in Linear Filtering and Prediction Theory," *Journal of Basic Engineering*, Vol. 83, 1961, pp. 95–108.

[13]Kitada, Y., "Identification of Nonlinear Structural Dynamic Systems Using Wavelets," *Journal of Engineering Mechanics*, Vol. 123, No. 10, 1998, pp. 1059–1066.

[14]Levy, E. C., "Complex Curve Fitting," *Institute of Electrical and Electronics Engineers Transactions on Automatic Control*, Vol. AC-4, 1959, pp. 37–43.

[15]Wellstead, P. E., Edmunds, J. M., Prager, D., and Zanker, P., "Self-Tuning Pole/Zero Assignment Regulators," *International Journal of Control*, Vol. 30, 1979, pp. 1–26.

[16]Coppolino, R. N., "A Simultaneous Frequency Domain Technique for Estimation of Modal Parameters from Measured Data," *Society of Automotive Engineers Transactions*, Paper 811046, 1981.

[17]Van der Auweraer, H., and Leuridan, J., "Multiple Input Orthogonal Polynomial Parameter Estimation," *Mechanical Systems and Signal Processing*, Vol. 1, No. 3, 1987, pp. 259–272.

[18]Ebersbach, P., and Irretier, H., "On the Application of Modal Parameter Estimation Using Frequency Domain Algorithms," *Journal of Analytical and Experimental Modal Analysis*, Vol. 4, No. 4, 1989, pp. 109–116.

[19]Craig, R. R., Kurdila, A. J., and Kim, H. M., "State-Space Formulation of Multi-Shaker Modal Analysis," *Journal of Analytical and Experimental Modal Analysis*, Vol. 5, No. 3, 1990, pp. 169–183.

[20]Mayes, R. L., and Johansen, D. D., "A Modal Parameter Extraction Algorithm Using Best-Fit Reciprocal Vectors," *Proceedings 16th International Modal Analysis Conference*, Society of Experimental Mechanics, Santa Barbara, CA, 1998, pp. 517–521.

[21]Katafygiotis, L. S., Papadimitriou, C., and Lam, H. F., "A Probabilistic Approach to Structural Model Updating," *Journal Soil Dynamics & Earthquake Engineering*, Vol. 17, No. 7–8, 1998, pp. 495–507.

[22]Lutes, L. D., and Sarkani, S., *Stochastic Analysis of Structural and Mechanical Vibrations*, Prentice–Hall, Upper Saddle River, NJ, 1997.

[23]Yaglom, A. M., *Correlation Theory of Stationary and Related Random Functions*, Vol. 1, Prentice–Hall, Upper Saddle River, NJ, 1987.

[24]Krishnaiah, P. R., "Some Recent Developments on Complex Multivariate Distributions," *Journal of Multivariate Analysis*, Vol. 6, 1976, pp. 1–30.

[25]Brillinger, D. R., *Time Series, Data Analysis and Theory*, Holt, Rinehart, and Winston, Philadelphia, 1975.

[26]Schoukens, J., and Pintelon, R., *Identification of Linear Systems: A Practical Guideline for Accurate Modeling*, Pergamon, London, 1991.

[27]Katafygiotis, L. S., and Yuen, K. V., "Statistical Modal Identification Using Ambient or Strong Wind Response Data," *Proceedings 4th International Conference on Stochastic Structural Dynamics*, Univ. of Notre Dame, Notre Dame, IN, 1998, pp. 387–394.

[28]Katafygiotis, L. S., Papadimitriou, C., and Yuen, K. V., "An Optimal Sensor Location Methodology for Designing Cost-Effective Modal Experiments," *European Dynamic Conference 99*, A. A. Balkema, Prague, 1999, pp. 617–622.

[29]Papadimitriou, C., Beck, J. L., and Au, S. K., "Entropy-Based Optimal Sensor Location for Structural Model Updating," *Journal of Vibration and Control*, Vol. 6, No. 5, 2000, pp. 781–800.

A. Berman
Associate Editor